EXPERIMENTAL INVESTIGATION INTO THE MECHANICAL BEHAVIOR OF TEXTILE COMPOSITES WITH VARIOUS FIBER REINFORCEMENT ARCHITECTURES

V. Khatkar,[1*] A. G. Sakthi Vijayalakshmi,[1] R. N. Manjunath,[2] S. Olhan,[1] and B. K. Behera[1]

The role of fiber reinforcement architecture in adjusting the mechanical properties of glass-fiber-reinforced epoxy composite materials is studied. Fibrous E-glass unidirectional (UD) and 3-dimensional (3D) samples with an identical fiber volume fraction were prepared. The UD composites displayed excellent properties along the fiber direction, but the 3D ones showed excellent properties in all three directions. The high delamination and impact resistances were additional advantages of 3D-reinforced composites to choose them as reliable materials for structural applications.

1. Introduction

Advancements in composite processing and their reinforcement architecture have resulted in new applications of composite materials in lightweight and high-strength systems. Fiber-reinforced composite materials offer a higher specific strength and stiffness than the conventional engineering materials [1]. They are employed in today's automotive, aerospace, and marine, sports, and power sectors [2-7]. Genovese et al. [2] investigated the mechanical properties of composites for railway application. Kumar and Das [3] examined the suitability of biocomposites made from nettle and PLA fibers for automotive dashboard applications. Belingardi et al. [4] studied alternative lightweight materials for the frontal bumper beam of vehicles. Khatkar and Behera [5] experimentally investigated composite leaf springs with various fiber reinforcement architectures. Wang et al. [6] and Ullah et al. [7] investigated the dynamic behavior of textile-based composites used for sports products. Manjunath and Behera [8] was engaged in modelling the geometry of the unit cell of woven fabrics with integrated stiffener sections for marine

[1]Department of Textile Technology, Indian Institute of Technology Delhi, New Delhi-110016, India
[2]Central Muga Eri Research & Training Institute, Central Silk Board, Jorhat Assam-785700
[*]Corresponding author; e-mail: vikas.khatkar1989@gmail.com

applications. Manjunath et al. [9] investigated the influence of augmented tuning of core architecture in 3D-woven sandwich composite structures on their flexural and compression behavior. Santos et al. [10] analyzed the use of metal fiber laminates for aerospace applications. The properties of fiber-reinforced composite materials greatly depend on the geometrical arrangement of fibers and their interaction with the matrix [11]. Textile fibers in the form of cut staples have been used over many decades to produce reinforced composites. In order to optimize the internal geometry of reinforcement structure for specific applications, it is necessary to understand how this structure affects the mechanical properties of composites. Textile-reinforced composites are traditionally produced by laminating unidirectional (UD) and bidirectional (2D) preforms when a high thickness is required for load-bearing structures. Several investigations have been carried out into the mechanical behavior of UD and 2D laminated composites. Priyanka et al. [12] presented a review of hybrid textile composites (carbon, glass, and aramid) meant for impact-resistant structures. Lobanov and Slovikov [13-14] investigated the mechanical behavior of basalt-reinforced unidirectional (UD) composites under thermomechanical loadings. Bidirectional (2D) textile preforms as a reinforcement for laminated composites are normally produced by weaving, knitting, braiding, or using a nonweaving technique [15-16]. The common failure mode in laminated composite structures is delamination under the action of various mechanical stresses [17-18]. Different techniques have been proposed to deal with the delamination problem. Shang et al. [19] put forward a technique to control the delamination of adhesively bonded joints of composite layers. Integrated three-dimensional (3D-woven) preforms having three series of yarn systems disposed in three mutually perpendicular directions can be a remedial solution to overcome delamination issues [20-21]. Turner et al. [22] studied 3D composites for their inplane tensile/compression and out-of-plane bending and found that they exhibited a significantly higher delamination resistance than UD laminates having of similar fiber volume fraction. Composites reinforced with a 3D woven fabric structures (orthogonal fabrics in particular) demonstrate a superior energy absorption capacity and impact damage resistance in comparison with unidirectional (UD) and 2D woven composites at a comparable fiber volume fraction [23-27]. Guénon et al. [23] investigated the toughness of 3D carbon fiber-epoxy composites and found that through-thickness reinforcement increased the interlaminar toughness up to 10 times and by about 25% increased the in-plane fracture toughness. Tanzawa et al. [24-25] carried out an experimental study on 3D woven orthogonal and interlock-based composites to clear up their delamination and fracture toughness. Behera and Das [26] studied the mechanical behavior of 3D-woven fabrics for their applicability to structural composites. Zhang et al. [27] investigated the low-speed impact behavior of fabric-reinforced composite laminates.

Warren et al. [28] carried out a mechanical analysis of composites with three different 3D fiber architectures and compared them with 2D woven ones. Their tensile, compressive, and in-plane shear properties were examined. Various investigations have also been carried out on the mechanical behavior of 3D woven composite [29-33]. The effect of binder configuration on their tensile properties and loading-direction-sensitivity were also studied by some researchers [28-29]. Topal et al. [31], Dinget et al [32] and Carvelli et al. [33] investigated the fatigue behavior of 3D woven composites. In the light of all these research works, it becomes clear that a further development of reinforcement engineering is possible only by clarifying how the reinforcement architecture affects the properties of composites. Some investigations have also shown the contribution reinforcement to the total load-bearing capacity of a structural composite reaches almost 90% if the internal geometry of architecture of the textile material is properly designed. In order to analyze this fact, composite panels with various textile reinforcement structures, from simple cut staple fibers to complex 3D woven structures in a resin system, were examined for their mechanical behavior under various loading conditions.

2. Materials and Methods

2.1. Materials

Continuous multifilament E-glass tows (supplied by Owens Corning, India) with 300, 1200, and 2400 tex (linear density) were used for the preparation of 2D and 3D fabric preforms. The same tow was cut into staples of length 25 mm for chopped fibers and was also used in a continuous form for UD reinforced composites. Figure 1 shows the different
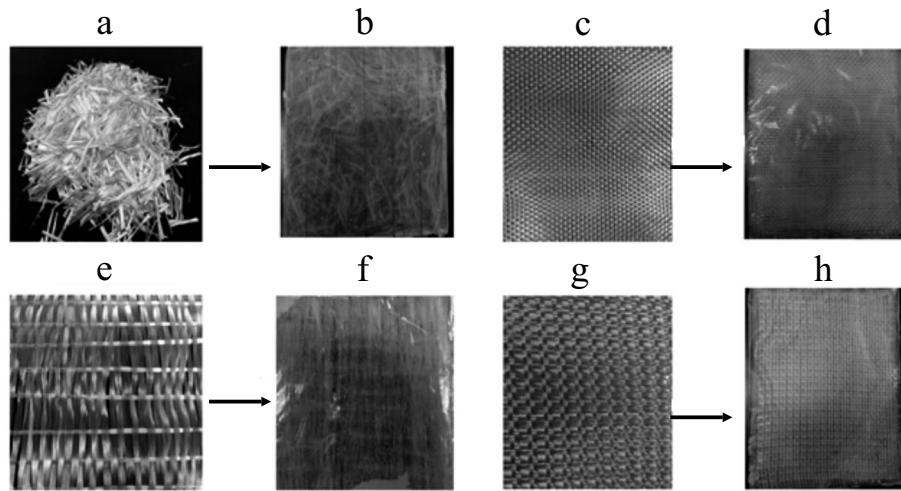
Fig. 1. Photograph of different reinforced composite samples: chopped fibers (a), chopped-fiber composite (b), 2D plain fabric (c), 2D composite (d), UD fabric (e), UD composite (f), 3D fabric (g), and 3D composite (h).
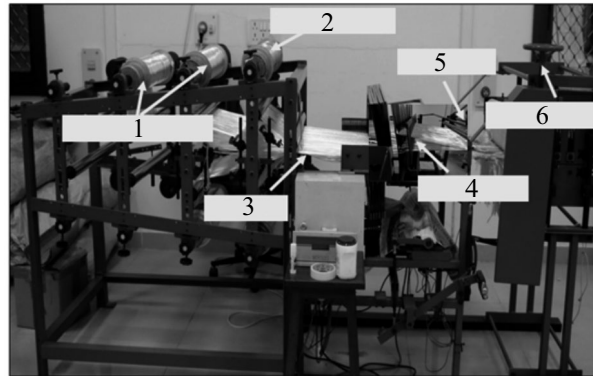

Fig. 2. Rigid rapier multibeam weaving machine: 1 — main wrap yarn beam, 2 — binder yarn beam, 3 — warp sheet, 4 — shed formation, 5 — woven fabric, and manual take-up.

reinforced composite structures considered. The tensile strength, elongation, and elastic modulus of the glass fiber tow were found to be 3400 ± 15 MPa, 2.50 ± 12%, and 70 ± 1.4 GPa, respectively. The matrix used for the fabricating composites was a mixture of an epoxy resin (Supplied by Northern Polymers Pvt. Ltd. (Delhi) India) of grade LY 556 and a hardener grade HY 917 in the mass ratio of 10:1. The tensile strength, elongation, and elastic modulus of epoxy were 71 ± 1.5 MPa, 4.2 ± 0.12%, and 4.8 ± 0.21 GPa, respectively.

2.2. Methods

2.2.1. Reinforcement development. Plain woven (2D) and 3D woven orthogonal fabric preforms were made using a rigid rapier multibeam sample weaving machine (Fig. 2), and their parameters indicated in Table 1. The peg plan and cross section of 2D plain weave and 3D orthogonal weave are shown in Fig. 3. In the 3D orthogonal weave architecture three, yarns (two warp and one weft yarns) are disposed in three mutually perpendicular directions. One extra binder warp beam was required for the through-thickness reinforcement, but only one warp beam was used for the 2D plain weave, because yarns were interlaced only in the warp and weft directions. The 3D-orthogonal weave architecture was created on the same

TABLE 1. Structural Parameters of UD, 2D, and 3D Fabric Preforms

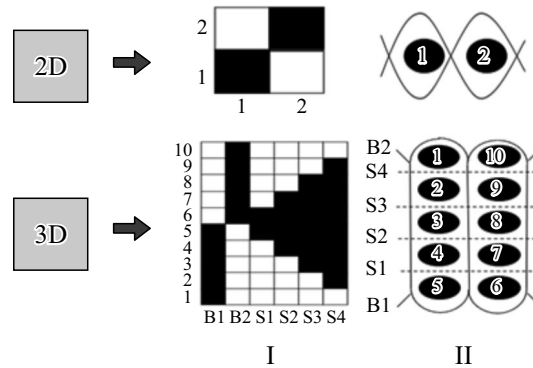| Fabric preform	Tow linear density, tex			Amount of ends/m			Reed count, (dents/2 inch)	Denting order (Stuffer (S): Binder (B))	Width of fabric, m
	Stuffer	Filler	Binder	Stuffer	Filler	Binder			
UD	1200	—	—	394	78	—	20	1:1	0.4
2D	1200	2400	—	394	433	—	20	1:1	0.4
3D	1200	2400	300	1184	1260	158	12	10:1	0.4

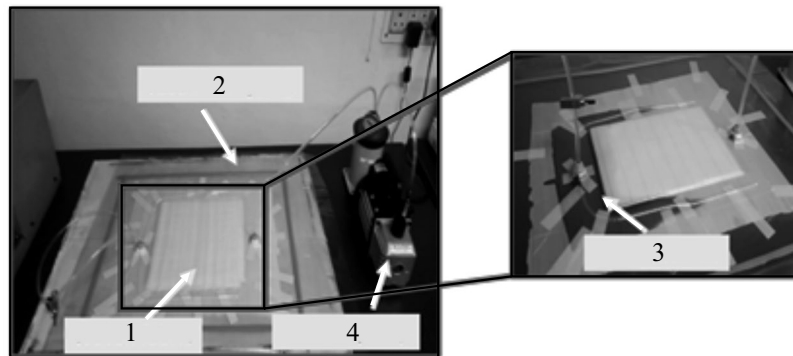Fig. 3. Flow chart of the reinforcement developed: I — peg plan and II — cross section.

Fig. 4. Vacuum-assisted resin infusion molding (VARIM): 1 — woven fabric, 2 — vacuum bagging, 3 — resin infusion, and 4 — vacuum pump.

machine. A four-layer 3D orthogonal weave with 6108 ± 160 GSM was developed using one beam for the binder warp and four beams for the main warp. Separate beams were used for the stuffer (warp) yarns and binder yarns. In order to compare the mechanical properties of textile-reinforced composites, the areal density (GSM) of the reinforcement architecture should be maintained constant. Therefore, a five-ply laminate of 2D plain weave fabric and a nine-ply unidirectional (UD) laminate were used to obtain an equivalent to the 3D orthogonal woven fabric. The same amount of chopped fibers of cut staple of length 25 mm were used for the development of chopped-fiber-reinforced composites.

2.2.2. Composite manufacturing. All fabric preforms were converted to composites infusing an epoxy resin into them by the vacuum bagging technique. The vacuum-assisted resin infusion molding (VARIM) setup is shown in Fig. 4. The composites samples were cured at room temperature for 24 h. The unreinforced epoxy and chopped-fiber-reinforced

TABLE 2. Measured Parameters of Fabric Preforms and Composites

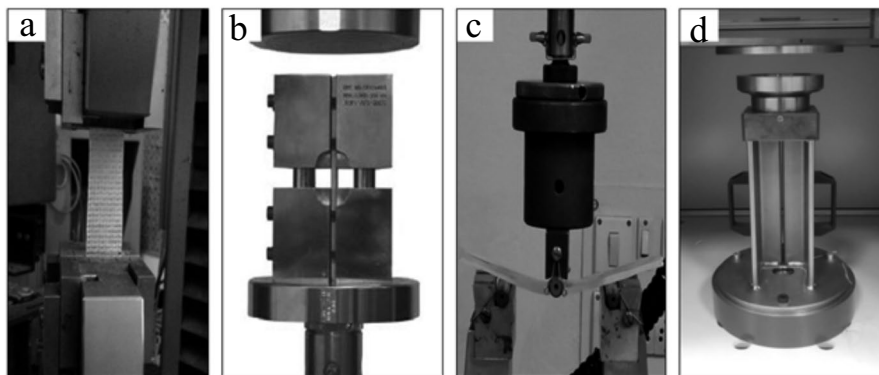| Composite	Number of layers	ρ_A. g/m^2	h. mm	V_f. %
Chopped	—	—	7.4±0.27	30±1.2
UD	9	6887±120	7.3±0.42	31±2.1
2D	5	6377±140	7.5±0.31	30±1.9
3D	1	6108±160	7.1±0.26	29±2.4

Fig. 5. Setups for tensile (a), compression (b), flexural (c), and drop-weight impact (d) tests.

composites were prepared placing the resin-fiber mixture in molds, applying a pressure to them with a hydraulic press, and curing for 24 h at room temperature. A constant fiber volume fraction (FVF) was maintained for all composites, which was determined using the density buoyancy method (Archimedes principle). The sample weight was first measured in air and then in distilled water. Knowing the specific gravity and the density of constituent materials, the fiber percentage was calculated. The results obtained were also validated employing a similar principle for volumes, measuring the increase in the volume of water when the fabric and the composite were immersed in it [28]. The stacking order, areal density (GSM), and FVF of all the samples are given in Table 2.

FVF is the parameter that quantifies the volume of fibers/reinforcing material present in composites, therefore, its optimization is very important in designing composite structures. In this study, all the composite structures were prepared with FVF = 30%.

2.2.3. Static mechanical analysis of composites. *2.2.3.1. Tensile test.* The tensile properties of composites were determined in accordance with the ASTM D 3039 standard. Test coupons of dimensions 250 × 25 mm with a gage length of 150 mm were prepared. Tests were carried out at a deformation rate of 2 mm/min using an INSTRON 5982 universal testing machine of capacity of 100 kN, and the average of five measured values was reported [34].

2.2.3.2. Compression test. The compressive properties were determined in accordance with ASTM D 3410 using a ZwickRoell 250 universal testing machine. Five measurements were recorded for each composite category. Sample dimensions were 135 × 25 mm, the gage length was 25 mm, and the crosshead motion rate was 1.5 mm/min. The average thickness of samples was 7 mm, and they were fastened in wedge grips using a specially designed fixture [35].

2.2.3.3. Flexural test. The flexural properties were determined in three-point bending in accordance with the ASTM D 7264 standard. Test coupons of dimensions 120 × 19 mm with a span-to-thickness ratio 16:1 were prepared. The gage length was 80 mm. The tests were conducted at a deformation rate of 1 mm/min on an INSTRON 5982 universal testing machine with a load cell capacity of 10 kN [36].

2.2.3.4. Low-speed impact test. The impact properties were determined in accordance with the ASTM D7136 standard. Test specimens of dimensions 120 × 120 mm were prepared from composite plates. A CEAST 9350 drop tower
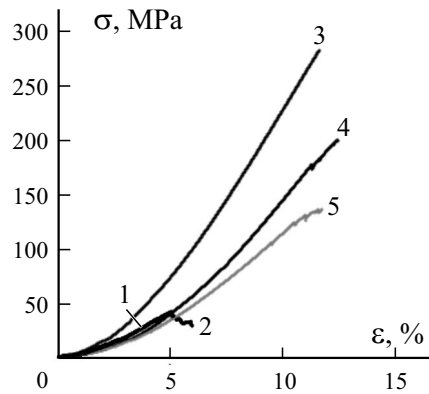
Fig. 6. Tensile stress–strain curves $\sigma - \varepsilon$ of matrix (1), chopped-fiber composite (2), and UD (3), 2D (4), and 3D (5) composites.

of capacity 400 J was used for testing their low-speed impact properties. A hemispherical impactor was allowed to drop at a speed of 4.5 m/s. The hemispherical impactor generates a higher amount of internal damage than the conical one. Since our objective was to determine the delamination (internal) failure of the composites, we used a hemispherical one. Alternative impactors (flat and conical) may be appropriate for examining the damage resistance. For example, a sharp striker may be better if the penetration resistance has to be assesed [37]. The experimental setups used for the mechanical tests are shown in Fig 5.

3. Results and Discussion

3.1. Tensile properties of composites

Figure 6 shows the typical experimental stress–strain curves, but the measured mechanical characteristics are summarized in Table 3. As is seen, the UD composite had the highest tensile strength, but the unreinforced epoxy — the lowest one. The strengths of remaining reinforced materials were between these two. The UD composite had the highest ultimate strength for the obvious reason — all its fibers were present in one direction and contributed to its load-bearing capacity during tensile loading. But in the 2D and 3D composites, the fibers were distributed in two and three directions, and their load-bearing capability was shared in two and three different directions, respectively. This is the potential advantage of textile structures, which facilitates a controlled distribution of constituent fibers in any desired direction during manufacturing preforms. Another important observation deserving attention is the fact that the failure modes of fiber-reinforced composites are characterized by matrix cracking, crack propagation, and delamination (separation of layers). A microscopic analysis was carried out to clear up the true cause of failure for all the reinforced composites considered. Figure 7 shows the microscopic images (side view) of tensile fractured specimens. The microscopic observation of fractured samples revealed that chopped-fiber-reinforced composite underwent a random failure, the UD and 2D composites failed by delamination (separation of stacked layers), but the 3D composites suffered a sharp breakage in the transverse direction, typically at the center, showing balanced and isotropic behavior, almost without any delamination. This means that 3D woven structure secures a stable composite material with uniform stress concentrations. In the case of UD and 2D composites, it is difficult to reach a higher thickness and areal density for woven preforms by the conventional weaving; therefore, the traditionally multilayering by stitching or adhesive bonding was used. But the 3D weaving is without this limitation, which facilitates the production of integrated heavy structures both in terms of thickness and areal density and prevents delamination.
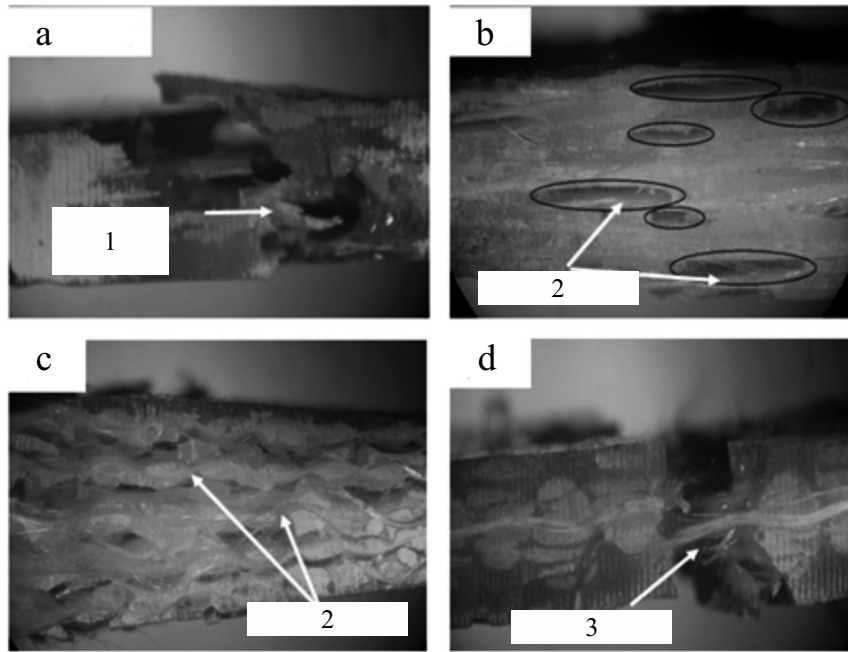
Fig. 7. Microscopic images (side view) of tensile fracture of chopped-fiber composite (a), and UD (b), 2D (c), and 3D (d) composites: 1 — random failure, 2 — delamination, and 3 — sharp brekage.

TABLE 3. Tensile E^t and Compressive E^c Young's Moduli, Tensile σ^{tu} and Compressive σ^{cu} Strengths, and the Ultimate Strain ε^{tu} of Materials

Material	σ^{tu}, MPa	E^t, GPa	ε^{tu}, %	σ^{cu}, MPa	E^c, GPa
Epoxy	55±2.1	0.14±0.012	7.8±0.40	39±1.7	0.98±0.023
Chopped-fiber	70±1.6	0.29±0.023	6.2±0.23	108±3.2	2.2±0.05
UD	256±3.0	0.26±0.015	11±0.69	200±3.4	1.9±0.01
2D	167±4.4	0.27±0.013	9.2±0.57	84±2.1	2.0±0.02
3D	121±3.7	0.20±0.010	8.8±0.82	153±4.1	2.6±0.07

3.2. Compressive properties

The typical compressive stress–strain curves and the common failure modes observed during the compression test are shown in Fig. 8, but the mechanical characteristics for various reinforced composites are summarized in Table 3. As is seen, the highest compressive strength, equal to 200 ± 3.4 MPa, showed the UD composite, followed by the 3D, chopped-fiber, and 2D ones and the unreinforced epoxy. The strength of the 3D composite was lower than that of UD one, but the highest among all other composites, owing to the binding effect of the through-thickness yarns, which prevented the filler and warp yarns from buckling and, hence, excluded the delamination failure. The strength of the chopped-fiber composite was higher than that of the 2D one. This could be attributed to the presence of a high numbers of fiber ends, which could create an additional drag during the in-plane compression, but the 2D strength was lower due to the inherent crimp inside the plain weave (2D), which led to the delamination failure of 2D composites.

The most common failure modes observed during in the plain compression test were the transverse shear at the grip and top (TS), brooming at the middle of gage length (B), through-thickness shear (TTS), and splitting (S). Some failed composite samples are shown in Fig. 9.
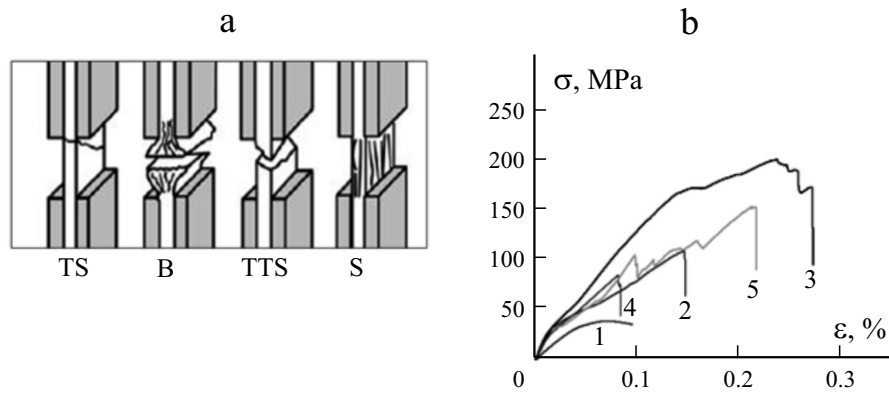
Fig. 8. Typical failure modes (a) and compression stress–strain curves $\sigma - \varepsilon$ of epoxy resin (1), of composite with chopped fibers (2), and of UD (3), 2D (4), and 3 D(5) composites (b). Explanations in the text.
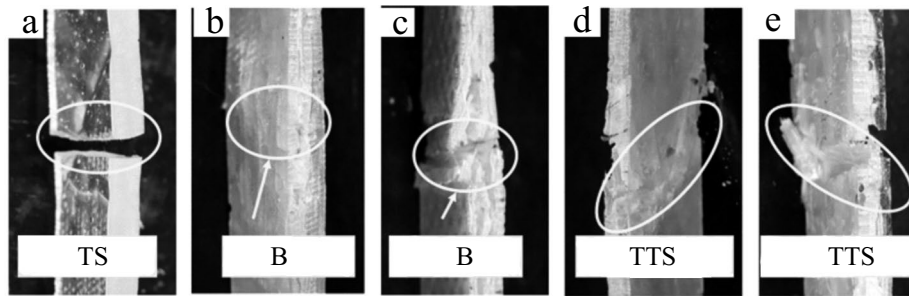

Fig. 9. Photographs of compression-fractured epoxy (a) and UD (b), 2D (c), chopped-fiber (d), and 3D composites (e). Explanations in the text.
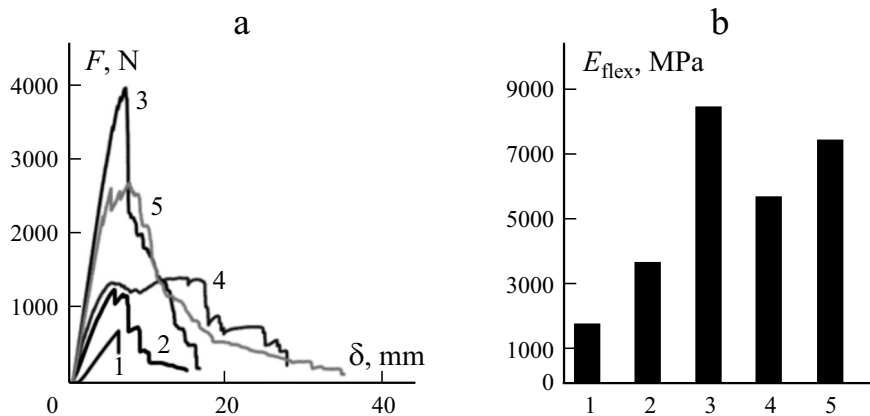

Fig. 10. Load–deflection curves $F - \delta$ ofmatrix (1), chopped-fiber composite (2), and UD (2), 2D (3), and 3D (5) composites (a) and diagrams of flexural rigidity (b).

3.3. Flexural (three-point bending) properties of composites

Figure 10a shows the typical load–deflection curves $F - \delta$ obtained in flexural tests. The flexural strength of the UD composite was the highest, 333± 4.2 MPa, — by about 67, 63, and 25% higher than those of chopped-fiber, 2D, and 3D composites. Figure 10b compares the flexural rigidities E_{flex} of composites with different reinforcement architectures.
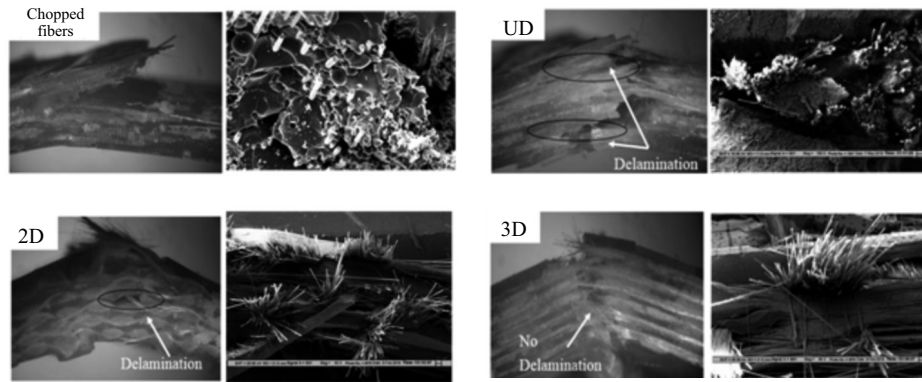
374

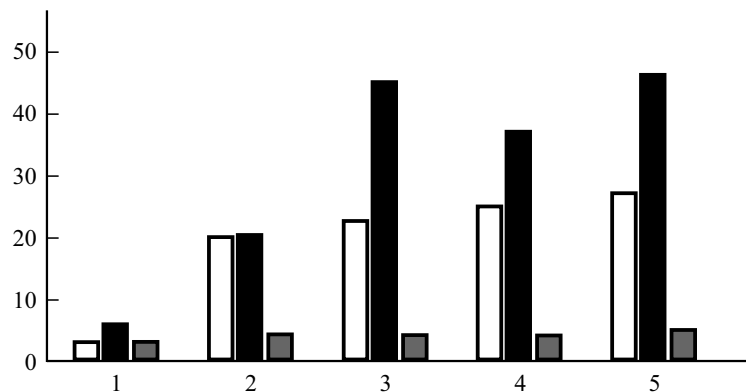Fig. 11. Microphotos and SEM images of raptured flexural specimens.

Fig. 12. Peak energy in J (■), damage force in N (□), and peak deformation in mm (■) of different composites. Designations as in Fig 10.

They can be arranged in the decreasing order UD > 3D >2D>chopped-fiber> epoxy. It is interesting to note that the UD composites exhibited a 23% higher flexural rigidity than the 3D one. The flexural rigidity of 3D was higher than that of 2D composites, with no signs of delamination (layer separation) on visual examination of ruptured samples. But significant amounts of delamination were seen on the UD and 2D composites. A further microscopic analysis was carried out to clear up the delamination problem. Figure 11 shows the microscopic images of ruptured samples. It is clearly seen the microscopic that delamination problems are significant for UD and 2D composites, but not for 3D ones.

3.4. Low-speed impact behavior of composites

Figure 12 compares the peak energy, damage force, and peak deformation of composites with various reinforcement architectures. The composite were tested at impact speeds of 4.5 to 5 m/s. The peak energy of the 3D composite was by about 7, 15, 26, and 89% higher than those of 2D, UD, and chopped-fiber composites and the unreinforced epoxy, respectively. As seen in Fig. 13, the unreinforced epoxy samples broke into multiple pieces like a brittle material while the chopped-fiber-reinforced composite was penetrated by the indenter completely. In UD and 2D composites, and opaque region formed around the impacted zone, which could be caused by delaminations (internal damage). A similar pattern was also observed by Das and Behera [11], which also was considered as a delamination. The 3D composite showed the highest energy absorption, with the smallest penetration depth and almost no delamination.
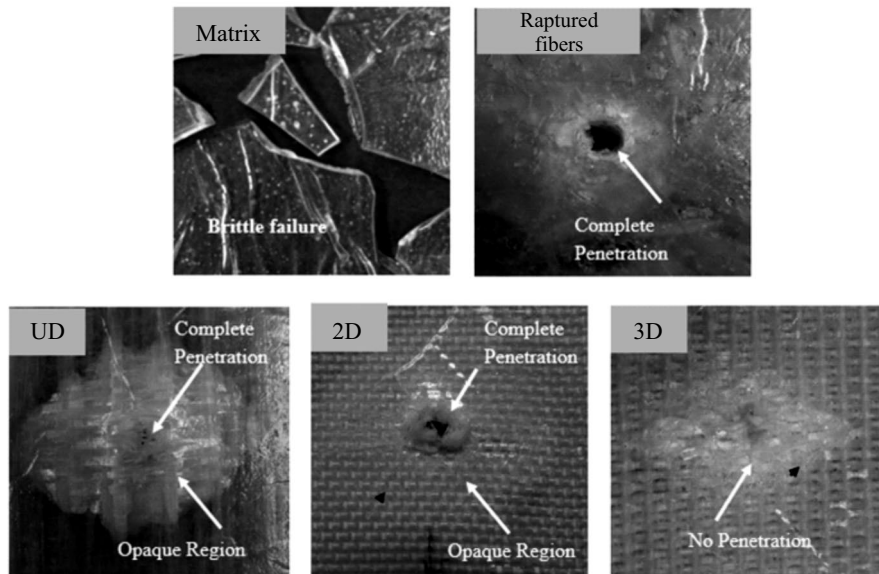
Fig. 13. Impact-tested specimens of different reinforced composites.

4. Conclusions

In this work, a comparative investigation of the mechanical properties of glass-epoxy composites with various reinforcement architectures has been performed. The study was focused mainly on the role of reinforcement material of fibrous, unidirectional and 3-dimensional formats in the behavior of composites under tensile, compressive, flexural, and impact loadings. The main findings of this work can be summarized as follows.

The tensile strength of the composites were found to decrease in the order UD> 2D> 3D> chopped-fiber> unreinforced epoxy. The availability of unidirectionally aligned fibers along the load bearing direction could be the main reason behind the performance of UD composites.

• The UD and 2D composites failed by delamination (internal damage), while the 3D ones displayed a high delamination resistance and a balanced and isotropic failure mode.

• The compressive and flexural strengths of 3D composites exceeded those of 2D composites, but UD and chopped-fiber composites and unreinforced epoxy showed similar trends.

• The flexural rigidities decreased in the order UD> 3D> chopped-fiber> 2D> unreinforced epoxy.

The final conclusion is that, by their mechanical characteristics, glass-epoxy composites with a 3D reinforcement exceed those with other reinforcement architectures.

REFERENCES

1. P. K. Mallick, Fiber-Reinforced Composites: Materials, Manufacturing, and Design, CRC press (2007).
2. A Genovese, M. Russo, and S. Strano, "Mechanical characterization and modeling of an innovative composite material for railway applications," Proceedings of the Institution of Mechanical Engineers, Part L: J. Mater. Des. Appl., **231**, No. 1, 2, 122-130 (2017)

3. N. Kumar and D. Das, "Fibrous biocomposites from nettle (Girardiniadiversifolia) and poly (lactic acid) fibers for automotive dashboard panel application," Compos. Part B, Eng., **130**, 54-63 (2017).

4. G. Belingardi, A. T. Beyene, E.G. Koricho, and B. Martorana, "Alternative lightweight materials and component manufacturing technologies for vehicle frontal bumper beam," Compos. Struct. **120**, 483-495 (2015).

5. V. Khatkar and B. K. Behera, "Experimental investigation of composite leaf spring reinforced with various fiber architecture," Adv. Compos. Mater., 1-17 (2019)

6. C. Wang, A. Roy, Z. Chen, and V. V. Silberschmidt, "Braided textile composites for sports protection: Energy absorption and delamination in impact modelling," Mater. Des., **136**, 258-269 (2017).

7. H. Ullah, A. R. Harland, and V. V. Silberschmidt, "Dynamic bending behaviour of woven composites for sports products: Experiments and damage analysis," Mater. Des., **88**, 149-156 (2015).

8. R. N. Manjunath, B. K. Behera, "Modelling the geometry of the unit cell of woven fabrics with integrated stiffener sections," J. Text. I. **108**(11), 2006-2012 (2017)

9. R. N. Manjunath, V. Khatkar, and B. K. Behera, "Influence of augmented tuning of core architecture in 3D woven sandwich structures on flexural and compression properties of their composites," Adv. Compos. Mater., 1-17 (2019).

10. D. G. dos Santos, R. J. C. Carbas, E. A.S. Marques, and L. F. M. da Silva, "Reinforcement of CFRP joints with fiber metal laminates and additional adhesive layers," Compos., Part B, Eng. **165**, 386-396 (2019).

11. B. K. Behera and B. P. Dash, "Mechanical behavior of 3D woven composites," Mater. Des., **67**, 261-71 (2015).

12. P. Priyanka, A. Dixit, and H. S. Mali, "High-strength hybrid textile composites with carbon, kevlar, and e-glass fibers for impact-resistant structures. A Review," Mech. Compos. Mater., **53**, No. 5, 685-704 (2017).

13. D. S. Lobanov and S. V. Slovikov, "Mechanical properties of a unidirectional basalt-fiber-reinforced plastic under a loading simulating operation conditions," Mech. Compos. Mater., **52**, No. 6, 767-772 (2017).

14. D. S. Lobanov, and S. V. Slovikov, "Mechanical behavior of a unidirectional basalt-fiber-reinforced plastic under thermomechanical loadings," Mech. Compos. Mater., **54**, No. 3, 351-358 (2018).

15. R. N. Manjunath and B. K. Behera, "Modelling the geometry of the unit cell of woven fabrics with integrated stiffener sections," J. Tex. Inst., **108**, No. 11, 2006-12 (2017).

16. R. N. Manjunath and B. K. Behera, Emerging Trends in Three-Dimensional Woven Preforms for Composite Reinforcements, In: Shahid-Ul Islam, Butola B.S. (eds.) Advanced Textile Engineering Materials, Wiley USA, 463-97 Wiley, USA(2018).

17. H. Gu and Z. Zhili, "Tensile behavior of 3D woven composites by using different fabric structures,"Mater. Des., **23**, No. 7, 671-674 (2002).

18. B. K. Behera and B. P. Dash, "A study on structure property relationship of 3D woven composites," Mater Today Proc., **2**, No. 4, 5, 2991-3007 (2015).

19. X. Shang, E. A. S. Marques, J. J. M. Machado,R. J. C. Carbas, D. Jiang, and L. F. Mda Silva, "A strategy to reduce delamination of adhesive joints with composite substrates," Proceedings of the Institution of Mechanical Engineers, Part L: J. Mater. Des. Appl., **233**, No. 3, 521-530 (2019)

20. B. K. Behera and R. Mishra R, "3-Dimensional weaving," Indian J Fiber and Textile Research, **33** (2008).

21. R. Mishra, J. Militky, B. K. Behera, and V. Banthia, "Modelling and simulation of 3D orthogonal fabrics for composite applications," J. Text. Inst., **103**, No. 11, 1255-61 (2012).

22. P. Turner, T. Liu, and X. Zeng, "Collapse of 3D orthogonal woven carbon fiber composites under in-plane tension/ compression and out-of-plane bending," Compos. Struct., **142**, 286-297 (2016).

23. V. A. Guénon, T. W. Chou, and J. W. Gillespie, "Toughness properties of a three-dimensional carbon-epoxy composite," J. Mater. Sci., **24**, No. 11, 4168-75 (1989).

24. Y. Tanzawa and Y. Tanzawa, "Experimental study of interlaminar delamination toughness of 3-D orthogonal interlocked fabric composite," In38th Structures, Structural Dynamics, and Mater. Conference, 1294 (1997).

25. Y. Tanzawa, N. Watanabe, and T. Ishikawa, "Interlaminar fracture toughness of 3-D orthogonal interlocked fabric composites," Compos. Sci. and Technol., **59**, No. 8, 1261-70 (1999).

26. B. K. Behera and B. P. Dash, "An experimental investigation into the mechanical behavior of 3D woven fabrics for structural composites," Fibers Polym., **15**, No. 9, 1950-55 (2014)

27. D. Zhang, Y. Sun, L. Chen and N. Pan, "A comparative study on low-velocity impact response of fabric composite laminates," Mater. Des., **50**, 750-6 (2013).
28. K. C. Warren, R. A. Lopez-Anido, and J. Goering, "Experimental investigation of three-dimensional woven composites," Compos. Part A, Appl. Sci. Manuf., **73**, 242-259 (2015).
29. S. Dhiman, P. Potluri, and C. Silva, "Influence of binder configuration on 3D woven composites," Compos. Struct., **134**, 862-868 (2015)
30. M. N. Saleh, A. Yudhanto, P. Potluri, and G Lubineau, "Characterizing the loading direction sensitivity of 3D woven composites: Effect of z-binder architecture," Compos. Part A, Appl. Sci. Manuf., **90**, 577-588 (2016).
31. S. Topal, L. Baiocchi, A. D. Crocombe, and S. L. Ogin, "Late-stage fatigue damage in a 3D orthogonal non-crimp woven composite: An experimental and numerical study," Compos. Part A, Appl. Sci. Manuf., **79**, 155-163 (2015).
32. Y. Q. Ding, Y .Yan, R. McIlhagger, and D. Brawn, "Comparison of the fatigue behaviour of 2-D and 3-D woven fabric reinforced composites," J. Mater. Process Tech., **55**, No. 3, 4, 171-177 (1995).
33. V. Carvelli, G. Gramellini, S. V. Lomov, A. E. Bogdanovich, D. D. Mungalov, and I. Verpoest, "Fatigue behavior of non-crimp 3D orthogonal weave and multi-layer plain weave E-glass reinforced composites," Compos. Sci. Technol., **70**, No. 14, 2068-2076 (2010).
34. ASTM D. 3039/D 3039M-08. Standard Test method for Tensile Properties of Polymer Matrix Composite Materials," ASTM International, 100, 19428-2959 (2008).
35. ASTM, D. 3410/3410M-16: Standard Test Method for Compression Properties of Polymer Matrix Composite Materials with Unsupported Gage Section Shear Loading. ASTM International (2016).
36. ASTM D. 7264. Standard test method for flexural properties of polymer matrix composite materials. ASTM International (2015).
37. ASTM D. 7136/D 7136M-15. Standard Test Method for Measuring the Damage Resistance of a Fiber-Reinforced Polymer Matrix Composite to a Drop-Weight Impact Event. ASTM International (2015).